

A MONOLITHIC AND A PARTITIONED REDUCED BASIS METHOD FOR FLUID–STRUCTURE INTERACTION PROBLEMS

MONICA NONINO¹, FRANCESCO BALLARIN², AND GIANLUIGI ROZZA³

ABSTRACT. The aim of this work is to present a brief report concerning the various aspects of the Reduced Basis Method within Fluid–Structure Interaction problems. The idea is to adopt two different procedures and apply them to the same test case. First we perform a reduction technique that is based on a monolithic procedure, where we therefore solve all at once the fluid and the solid problem. Then we present an alternative reduction technique, that is based on a partitioned (or segregated) procedure instead: here the fluid and the solid problem are solved separately and then coupled through a fixed point strategy. The toy problem that we consider is the Turek–Hron benchmark test case, with a fluid Reynolds number $Re = 100$, which is known to lead to the formation of Karman vortices in the fluid, and a periodically oscillating behaviour in the structure.

1. INTRODUCTION

The bridging between approximation techniques and high performance computing finds a variety of different fields of applications, in the industry as well as in the academy: it is sufficient to think about heat transfer problems, electromagnetic problems, structural mechanics problems (linear/ nonlinear elasticity), fluid problems, acoustic problems. In all these examples, the models are described through a system of partial differential equations (PDE) that usually depends on a given number of parameters, that describe the geometrical configuration of the physical domain over which the problem is formulated, or they describe some physical quantities (e.g. the Reynolds number for a fluid or the Lamé constants for a solid), or some boundary conditions. For all these models we usually focus on a particular quantity of interest, also called output of interest, such as the maximum temperature of a system, a pressure drop, a channel flowrate. Unfortunately to compute such output for each new value of the parameter is a difficult task, that is expensive both in terms of time computation and in terms of computer memory, even on modern HPC systems. With these premises in mind, it is clear why the Reduced Basis Method [12, 29–31, 34, 39, 47] (RBM) comes into play and shows a wide range of advantages: the idea at the core of the method is to simulate the behaviour of the solution of our system of interest for some chosen values of the parameters in the PDE. This is usually done with some well established discretization technique, such as Finite Element Method (FEM); another discretization method, used for example in the compressible framework in computational fluid dynamics is the Finite Volume Method (FV), and yet another possibility is the CutFEM method (see for example [14, 15, 33]). Once we have computed these solutions, in an expensive offline phase, we can use them to build some other basis functions: with these new basis functions, in the inexpensive online phase, we approximate the solution of the system, for a new value of the parameter.

Among the various applications of the Reduced Basis Method, Fluid–Structure Interaction (FSI) problems definitely represent a great challenge as well as an extremely interesting topic. Indeed, despite their intrinsic complicated nature (see [19, 26]), FSI problems are frequently used: among some examples we have naval engineering, where they are used to study the

¹UNIVERSITY OF VIENNA, DEPARTMENT OF MATHEMATICS.

²CATHOLIC UNIVERSITY OF THE SACRED HEART, DEPARTMENT OF MATHEMATICS AND PHYSICS.

³SISSA, MATHEMATICS AREA, MATHLAB, INTERNATIONAL SCHOOL FOR ADVANCED STUDIES.

E-mail addresses: monica.nonino@univie.ac.at, fballarin@unicatt.it, grozza@sissa.it.

2010 *Mathematics Subject Classification.* 78M34, 97N40, 35Q35.

interaction between the water and the hull of a ship [37]; we can also have biomedical applications, where FSI problems are used to model the interaction between the blood flow and the deformable walls of a vessel ([7, 38, 42–44, 52, 52]); finally, in aeronautical engineering, FSI describes the way the air interacts with a plane or with (parts of) a shuttle, see [18, 20, 36, 45]. The goal of this work is to present a report concerning the performances of two different Reduced Basis Method approaches for Fluid–Structure Interaction (FSI) problems. The same test case is considered: the Turek–Hron benchmark test case, for which well established results and analysis are already present in the literature, see for example [48, 49].

The rest of the work is structured as follows: in Section 2 we briefly introduce the two main approaches that can be adopted when dealing with FSI, namely monolithic and partitioned approaches. In Section 3 we define the mathematical formalism behind coupled systems, and in particular we introduce the Arbitrary Lagrangian Eulerian (ALE) formulation. In Section 4 we present a monolithic reduced order model: in Section 4.1 we define the time discretization, in Section 4.2 we introduce the space discretization of the problem, and in Section 4.2.1 we discuss about the imposition of coupling conditions through Lagrangian multipliers. In Section 4.3 we introduce the supremizer enrichment technique, in Section 4.4 we formulate the online reduced order coupled system and finally in Section 5 we present some numerical results. Section 6 is devoted to a partitioned algorithm: in Section 6.1 and Section 6.2 we introduce the time discretization and the space discretization, respectively. In Section 6.3 we present the Proper Orthogonal Decomposition technique used in this case, and finally in Section 6.4 and 7 we present the online reduced order problem and some numerical results.

2. APPROACHES TO FLUID–STRUCTURE INTERACTION PROBLEMS

As we previously mentioned FSI problems are characterized by the presence of two very different physics, interacting with one another: we have the fluid problem, represented by the Stokes or Navier–Stokes equation, and we have the structure problem, represented by a string equation, by linear elasticity or by nonlinear elasticity. It is therefore almost natural to conclude that there are two main different routes one can take to address such problems. Indeed we can decide to solve separately the fluid and the solid problem, and then take care of the coupling between the two physics: this way of proceeding gives rise to the so called partitioned, or segregated, approach. On the other hand we can decide to solve together the two problems, and this gives rise to a monolithic procedure instead.

2.1. Monolithic approach. As we have said, in a monolithic algorithm the fluid and the solid problem are solved simultaneously. These kind of algorithms are more stable, and they usually allow the use of bigger time steps during the discretization in time of the problem. The main drawback is that one really relies on available ad hoc softwares that are capable of handling at the same time a computational fluid dynamics problem as well as a solid mechanics problem. In addition to this, in order to pursue a Galerkin discretization of the original problem, one needs to introduce Lagrange multipliers to impose the coupling conditions at the fluid–structure interface, thus increasing the number of unknowns in the coupled problem. For the reader interested in looking in more detail into monolithic algorithms, we refer to [6, 9, 24, 25, 40, 46, 53], even though this list is by no means complete.

2.2. Segregated approach. The rationale behind a partitioned approach is to deal separately with the two physics: this indeed allows to better exploit existing simulation tools for fluid dynamics and for structural dynamics, which are well developed nowadays and are used on a daily basis in industrial applications. A partitioned approach has many advantages: indeed we have the possibility to combine different discretization tools for the two physics (e.g. Finite Volumes for the fluid and Finite Elements for the structure), we have the possibility to refine in time for one of the two physics, if the situation requires to. Unfortunately also in this case there are some drawbacks, as it turns out that, under some physical and geometrical conditions, partitioned algorithms are unstable; this situation may occur when the physical domain has a slender shape, or when the fluid density ρ_f is close to the solid density ρ_s (this

is almost always the case in haemodynamics applications, where the density of the blood is quite close to the density of the walls of the vessel). This instability occurs because of the well known *added mass effect*: the fluid acts like an added mass to the solid, thus changing its natural behaviour. The reader interested in the analysis behind the added mass effect and in its derivation is referred to [16]. With a partitioned procedure we can give rise to a variety of different algorithms, according to the strategy used to impose the coupling conditions at the fluid–structure interface:

- *Explicit algorithms*: after time discretization, the coupling conditions are treated explicitly at every time–step. These algorithms, also known as *weakly* or *loosely* coupled algorithms [13], are successfully applied in aerodynamics applications, see [21, 41], but some studies (see [16, 32, 35]) showed that they are unstable under some physical and geometrical conditions, due to the added mass effect, as we previously mentioned.
- *Implicit algorithms*: in these algorithms, also known as *strongly* coupled algorithms, the coupling conditions are treated implicitly at every time–step, see for example [50, 51]. This implicit coupling represents a way to circumvent the instability problems due to the added mass effect; nevertheless, an implicit treatment of the coupling conditions leads to algorithms that are more expensive in terms of computational time.
- *Semi–implicit algorithms*: in these algorithms (see [4, 5, 11]), the continuity of the displacement is treated explicitly, whereas the other coupling conditions are treated implicitly. This alternative represents a tradeoff between the computational cost of the algorithm and its stability in relation to the physical and geometrical properties of the problem. In Section 6.4 we will see a reduced order method that is based on this kind of partitioned approach.

3. FLUID–STRUCTURE INTERACTION PROBLEMS

In the following we are going to introduce the mathematical formalism connected to multiphysics problems: we assume to be in a two dimensional setting, therefore let $\Omega(t) \subset \mathbb{R}^2$ be the physical domain of interest, at time $t \in [0, T]$. The physical domain can be naturally divided into two subdomains: $\Omega(t) = \Omega_f(t) \cup \Omega_s(t)$, where $\Omega_f(t)$ is the fluid domain, and $\Omega_s(t)$ is the solid domain; we further assume that $\Omega_f(t) \cap \Omega_s(t) = \emptyset$, and $\bar{\Omega}_f(t) \cap \bar{\Omega}_s(t) = \Gamma_{FSI}(t)$ is the fluid–structure interface.

The fluid is assumed to be newtonian and incompressible, and therefore its behaviour can be modelled through the incompressible Navier–Stokes equation: for every $t \in [0, T]$, find $u_f(t): \Omega_f(t) \mapsto \mathbb{R}^2$, $p_f(t): \Omega_f(t) \mapsto \mathbb{R}$ such that:

$$(1) \quad \begin{cases} \rho_f(\partial_t u_f + (u_f \cdot \nabla)u_f) - \operatorname{div} \sigma_f(u_f, p_f) = b_f & \text{in } \Omega_f(t) \times (0, T], \\ \operatorname{div} u_f = 0 & \text{in } \Omega_f(t) \times (0, T], \end{cases}$$

where $\sigma_f(u_f, p_f)$ is the Cauchy stress tensor that, given the fluid is newtonian, can be expressed in the following way:

$$\sigma_f(u_f, p_f) = \rho_f \nu_f (\nabla u_f + \nabla^T u_f) - p_f \mathbf{I}.$$

Here \mathbf{I} is the 2×2 identity matrix, ρ_f is the fluid density and ν_f is the kinematic viscosity. The solid behaviour is described by a linear elasticity equation: for every $t \in [0, T]$, find the solid displacement $\hat{d}_s(t): \hat{\Omega}_s \mapsto \mathbb{R}^2$ such that:

$$(2) \quad \partial_{tt} \hat{d}_s - \operatorname{div} \hat{P}(\hat{d}_s) = \hat{b}_s \quad \text{in } \hat{\Omega}_s \times (0, T],$$

where \hat{b}_s is the external force acting on the solid. We assume here to work with St.Venant Kirchhoff material: this means that the solid Piola–Kirchhoff stress tensor $\hat{P}(\hat{d}_s)$ can be expressed as

$$\hat{P}(\hat{d}_s) = 2\mu_s \varepsilon(\hat{d}_s) + \lambda_s \operatorname{tr} \hat{\varepsilon}(\hat{d}_s) \mathbf{I},$$

with μ_s and λ_s being the Lamé constants of the material.

The first thing we notice, from (1) and (2), is that the two problems are formulated over two "different kind" of domains: indeed, the Navier–Stokes equation is formulated over a *time-dependent* domain $\Omega_f(t)$, whereas the linear elasticity equation is formulated over a *time-independent* domain $\hat{\Omega}_s$. This is a rather natural peculiarity of fluid–structure interaction problems, that arises from the different nature of the two problems involved. Solving a FSI problem in a time dependent domain can be extremely costly from a computational point of view, as it requires a remeshing at every timestep, in order to update the entire configuration. One possible alternative to avoid remeshing is to try instead to solve the problems in a reference configuration. For the solid problem, the definition of the reference configuration is quite easy and natural: indeed, we can say that the solid reference configuration $\hat{\Omega}_s$ is exactly the solid domain, undeformed: $\hat{\Omega}_s = \Omega_s(t = 0)$. For the fluid problem, defining a reference configuration is instead rather complicated, and not obvious at all. To this aim, we introduce the ALE map

$$\begin{aligned} \mathcal{A}_f(t): \hat{\Omega}_f &\mapsto \Omega_f(t) \\ \hat{x} &\mapsto x = \hat{x} + \hat{d}_f(t), \end{aligned}$$

which maps an *arbitrary* time independent fluid domain to the fluid current configuration. In (??) the *mesh displacement* $\hat{d}_f(t)$ at time t is defined as an extension to the whole domain $\hat{\Omega}_f$ of the solid deformation $\hat{d}_s(t)$. This extension can be carried out in different ways: we adopt here an harmonic extension:

$$\begin{cases} -\frac{1}{J}\hat{\Delta}\hat{d}_f = 0, & \text{in } \hat{\Omega}_f \times [0, T] \\ \hat{d}_f = \hat{d}_s, & \text{on } \hat{\Gamma}_{FSI} \times [0, T]. \end{cases}$$

Here J is defined as $J(t) := \det F(t)$, where $F(t)$ is the gradient of the ALE map $\mathcal{A}_f(t)$. From now on, in order to ease the notation, we will drop the time dependence of J and F . The reader interested in alternative ways on how to define the mesh displacement is referred to [46].

Thanks to the introduction of the ALE map, we can decide to take as arbitrary time independent fluid domain the domain at time $t = 0$, hence $\hat{\Omega}_f := \Omega_f(t = 0)$. After some computations (see for example [46]), we can reformulate the Navier–Stokes problem in the reference configuration: for every $t \in [0, T]$, find the fluid velocity $\hat{u}_f(t): \hat{\Omega}_f \mapsto \mathbb{R}^2$, the fluid pressure $\hat{p}_f(t): \hat{\Omega}_f \mapsto \mathbb{R}$ and the fluid displacement $\hat{d}_f(t): \hat{\Omega}_f \mapsto \mathbb{R}^2$ such that:

$$(3) \quad \begin{cases} \rho_f J (\partial_t \hat{u}_f + \hat{\nabla} \hat{u}_f F^{-1} (\hat{u}_f - \partial_t \hat{d}_f)) - \hat{\text{div}}(J \hat{\sigma}_f(\hat{u}_f, \hat{p}_f) F^{-T}) = b_f & \text{in } \hat{\Omega}_f \times (0, T], \\ \hat{\text{div}}(J F^{-1} u_f) = 0 & \text{in } \hat{\Omega}_f \times (0, T], \\ -\frac{1}{J} \hat{\Delta} \hat{d}_f = 0 & \text{in } \hat{\Omega}_f \times (0, T], \end{cases}$$

where now $\hat{\sigma}_f(\hat{u}_f, \hat{p}_f)$ is the fluid Cauchy stress tensor in the arbitrary reference configuration $\hat{\Omega}_f$:

$$\hat{\sigma}_f(\hat{u}_f, \hat{p}_f) := \rho_f \nu_f (\nabla u_f F^{-1} + F^{-T} \nabla^T u_f).$$

Together equations (3) and (2) form the coupled FSI problem, expressed in a time independent configuration. In order to have a coupled system we still need some coupling conditions, that describe the interaction between the two physics:

$$(4) \quad \begin{cases} d_f = d_s & \text{on } \Gamma_{FSI}(t) \times (0, T], \\ u_f = \partial_t d_f & \text{on } \Gamma_{FSI}(t) \times (0, T], \\ \sigma_f n = P_s n & \text{on } \Gamma_{FSI}(t) \times (0, T], \end{cases}$$

where n is the normal to the fluid–structure interface. The entire coupled system is then completed by some initial conditions and by some boundary conditions. In the following we

will work with these boundary conditions:

$$\begin{cases} u_f = \bar{u} & \text{on } \hat{\Gamma}_D^f \times (0, T], \\ d_s = 0 & \text{on } \Gamma_D^s \times (0, T]. \end{cases}$$

Remark: from now on, unless otherwise stated, we will assume that everything is formulated over the reference configuration. Therefore, in order to ease the notation, we drop the hat symbol over the variables.

4. MONOLITHIC APPROACH

In the following we propose a monolithic approach for coupled problems. As already mentioned in the introduction, a monolithic approach means that we are going to solve the fluid and the solid problem all together; as we will see in Section 4.2.1 this leads to a more subtle treatment of the coupling conditions at the fluid–structure interface; at the same time adopting a monolithic procedure allows us to have a better control on the global behaviour of the coupled system.

4.1. Time discretization. We discretize the time interval $[0, T]$ with equispaced time sample points, thus obtaining $\{0 = t_0, \dots, t_{N_T} = T\}$, where $t_i = i\Delta T$, and ΔT is the timestep chosen. In the following we will make use of the notation $f^i := f(t^i)$, for any given function f . We discretize the time derivatives in the fluid problem with a second order backward difference formula (BDF2):

$$D_t u_f^{i+1} = \frac{3}{2\Delta T} u_f^{i+1} - \frac{4}{2\Delta T} u_f^i + \frac{1}{2\Delta T} u_f^{i-1}.$$

Using a Newmark scheme for the solid problem, we can define the structure first and second order time derivatives $D_t d_s$ and $D_{tt} d_s$:

$$\begin{aligned} D_{tt} d_s^{i+1} &= \frac{1}{\beta\Delta T} (d_s^{i+1} - d_s^i) - \frac{1}{\beta\Delta T} D_t d_s^i - \left(\frac{1}{2\beta} - 1\right) D_{tt} d_s^i, \\ D_t d_s^{i+1} &= \frac{\gamma}{\beta\Delta T} (d_s^{i+1} - d_s^i) - \left(\frac{\gamma}{\beta} - 1\right) D_t d_s^i - \Delta T \left(\frac{\gamma}{2\beta} - 1\right) D_{tt} d_s^i, \end{aligned}$$

where the constants γ and β are chosen in order to ensure unconditional stability of the Newmark scheme, as suggested in [17].

4.2. Space discretization. We now introduce the discrete version of the original problem (2)-(3), from a monolithic point of view. Let us define the following function spaces:

$$\begin{aligned} V^f &:= \{u_f \in H^1(\Omega_f) \text{ s.t. } u_f = \bar{u} \text{ on } \Gamma_D^f\}, \\ V_0^f &:= \{v_f \in H^1(\Omega_f) \text{ s.t. } v_f = 0 \text{ on } \Gamma_D^f\}, \\ Q &:= \{q \in L^2(\Omega_f)\}, \\ E^f &:= \{d_f \in H^1(\Omega_f)\}, \\ E^s &:= \{d_s \in H^1(\Omega_s) \text{ s.t. } d_s = 0 \text{ on } \Gamma_D^s\}. \end{aligned}$$

We discretize in space the FSI problem, using the inf-sup stable pair $(V_h^f, Q_h) = (\mathbb{P}_2, \mathbb{P}_1)$ for the fluid velocity and the fluid pressure, and similarly for the space V_0^f . For the mesh displacement we use first order Lagrange Finite Elements obtaining the discrete space $E_h^f \subset E^f$; for the solid displacement we employ instead second order Lagrange Finite Elements, resulting in the discretized space $E_h^s \subset E^s$. The weak formulation of problem (2), (3) now reads: find $u_{f,h} \in V_h^f$, $p_{f,h} \in Q_h$, $d_{f,h} \in E_h^f$ and $d_{s,h} \in E_h^s$ such that for every $v_{f,h} \in V_h^f$,

$q_h \in Q_h$, $e_{f,h} \in E_h^f$ and $e_{s,h} \in E_h^s$:

$$(5) \quad \begin{cases} (\partial_{tt}d_{s,h}, e_{s,h})_{\Omega_s} + (P(d_{s,h}), \nabla e_{s,h})_{\Omega_s} - (P(d_{s,h})n_s, e_s)_{\Gamma_{FSI}} = (b_s, e_{s,h})_{\Omega_s}, \\ \rho_f J(\partial_t u_{f,h}, v_{f,h})_{\Omega_f} + \rho_f J(\nabla u_{f,h} F^{-1} u_{f,h}, v_{f,h})_{\Omega_f} - \rho_f J(\nabla u_{f,h} F^{-1} \partial_t d_{f,h}, v_{f,h})_{\Omega_f} + \\ + (J\sigma_f(u_{f,h}, p_{f,h})F^{-T}, \nabla v_{f,h})_{\Omega_f} - (J\sigma_f(u_{f,h}, p_{f,h})F^{-T} n_f, v_{f,h})_{\Gamma_{FSI}} = (b_f, v_{f,h})_{\Omega_f} \\ - (\operatorname{div}(JF^{-1}u_{f,h}), q_h)_{\Omega_f} = 0 \\ (\frac{1}{j}\nabla d_{f,h}, \nabla e_{f,h})_{\Omega_f} = (\frac{1}{j}\nabla d_{f,h} n_f, e_{f,h})_{\Gamma_{FSI}}. \end{cases}$$

In the previous system, n_f and n_s are the normals to the fluid–structure interface, outgoing the fluid domain and the solid domain respectively.

4.2.1. *Coupling conditions through Lagrange multipliers.* Let us analyze a little bit more into detail the boundary integrals appearing in system (5). From condition (4)₃ it is clear that we have to satisfy:

$$(P(d_{s,h})n_s, e_{s,h})_{\Gamma_{FSI}} = -(J\sigma_f(u_{f,h}, p_{f,h})F^{-T} n_f, v_{f,h})_{\Gamma_{FSI}}.$$

Now let us have a look at conditions (4)₁ and (4)₂. It is easy to see that, in the time–continuous regime, thanks to (4)₂, the following are equivalent:

$$d_{f,h} = d_{s,h} \text{ on } \Gamma_{FSI}, \quad \partial_t d_{s,h} = u_{f,h} \text{ on } \Gamma_{FSI}, \quad \partial_t d_{s,h} = \partial_t d_{f,h} \text{ on } \Gamma_{FSI}.$$

This equivalence does not hold anymore in general after time discretization, as one may choose different time integration schemes for the fluid and for the solid. In this work we choose to enforce weakly the two following conditions:

$$(6) \quad d_{f,h} = d_{s,h} \text{ on } \Gamma_{FSI}, \quad \partial_t d_{s,h} = u_{f,h} \text{ on } \Gamma_{FSI}.$$

In order to do so, let us introduce first the space $L := H^{-\frac{1}{2}}(\Gamma_{FSI})$, and let us consider a finite dimensional subspace $L_h \subset L$. Let us take a discretized Lagrangian multiplier field $\lambda_{u,h} \in L_h$, and its corresponding test function $\mu_{u,h} \in L_h$. We can then write

$$(\mu_{u,h}, u_{f,h} - \partial_t d_{s,h})_{\Gamma_{FSI}} = 0,$$

and, by identifying the Lagrange multiplier with the unknown surface traction, we can finally rewrite the surface integrals in (5)₁ and (5)₂ as:

$$\begin{aligned} -(P(d_{s,h})n_s, e_{s,h})_{\Gamma_{FSI}} &= -(\lambda_{u,h}, e_{s,h})_{\Gamma_{FSI}}, \\ -(J\sigma_f(u_{f,h}, p_{f,h})F^{-T} n_f, v_{f,h})_{\Gamma_{FSI}} &= +(\lambda_{u,h}, e_{s,h})_{\Gamma_{FSI}}. \end{aligned}$$

We treat similarly the continuity of the displacements at the interface: we take another Lagrangian multiplier field $\lambda_{d,h} \in L_h$, and its corresponding test function $\mu_{d,h} \in L_h$. We can then write

$$(\mu_{d,h}, d_{f,h} - d_{s,h})_{\Gamma_{FSI}} = 0,$$

and we identify now the Lagrange multiplier with the surface traction caused by the mesh displacement, thus we can rewrite the surface integral in (5)₄ as:

$$(\frac{1}{j}\nabla d_{f,h} n_f, e_{f,h})_{\Gamma_{FSI}} = (\lambda_{d,h}, e_{f,h})_{\Gamma_{FSI}}.$$

Finally therefore, after the space and the time discretization, our monolithic coupled system reads as follows: for every t^i , $i = 0, \dots, N_T$, find $u_{f,h}^{i+1} \in V_h^f$, $p_{f,h}^{i+1} \in Q_h$, $d_{f,h}^{i+1} \in E_h^f$, $d_{s,h}^{i+1} \in E_h^s$, $\lambda_{u,h}^{i+1} \in L_h$ and $\lambda_{d,h}^{i+1} \in L_h$ such that for every $v_{f,h} \in V_h^0$, $q_h \in Q_h$, $e_{f,h} \in E_h^f$, $e_{s,h} \in E_h^s$,

$\mu_{u,h} \in L_h$ and $\mu_{d,h} \in L_h$:

$$(7) \quad \begin{cases} (D_{tt}d_{s,h}^{i+1}, e_{s,h})_{\Omega_s} + (P(d_{s,h}^{i+1}, \nabla e_{s,h})_{\Omega_s} + (\lambda_{u,h}^{i+1}, e_s)_{\Gamma_{FSI}} = 0, \\ \rho_f J(D_t u_{f,h}^{i+1}, v_{f,h})_{\Omega_f} + \rho_f J(\nabla u_{f,h}^{i+1} F^{-1} u_{f,h}^{i+1}, v_{f,h})_{\Omega_f} - \rho_f J(\nabla u_{f,h} F^{-1} D_t d_{f,h}^{i+1}, v_{f,h})_{\Omega_f} + \\ + (J\sigma_f(u_{f,h}^{i+1}, p_{f,h}^{i+1})F^{-T}, \nabla v_{f,h})_{\Omega_f} - (\lambda_{u,h}^{i+1}, v_{f,h})_{\Gamma_{FSI}} = 0 \\ -(\operatorname{div}(JF^{-1}u_{f,h}^{i+1}), q_h)_{\Omega_f} = 0 \\ (\frac{1}{J}\nabla d_{f,h}^{i+1}, \nabla e_{f,h})_{\Omega_f} = (\lambda_{d,h}^{i+1}, e_{f,h})_{\Gamma_{FSI}}, \\ (u_{f,h}^{i+1} - D_t d_{s,h}^{i+1}, \mu_{u,h})_{\Gamma_{FSI}} = 0, \\ (d_{f,h}^{i+1} - d_{s,h}^{i+1}, \mu_{d,h})_{\Gamma_{FSI}} = 0. \end{cases}$$

4.3. Reduced Basis generation and supremizer enrichment. Once we have set the mathematical formalism and the space and time discretization, we can run the monolithic Finite Element solver for every timestep t^i , $i = 0, \dots, N_T$, and we then obtain the snapshots $(u_{f,h}^i, p_{f,h}^i, d_{f,h}^i, d_{s,h}^i, \lambda_{u,h}^i, \lambda_{d,h}^i)$. In order to ease the treatment of the non-homogeneous Dirichlet boundary condition for the fluid velocity, we introduce a lifting function $\ell_h \in V_h^f$; we then subtract the lifting function to the fluid velocity, obtaining a new variable $u_{0,h} := u_{f,h} - \ell_h$ that satisfies a homogeneous Dirichlet boundary condition at the fluid Dirichlet boundary Γ_D^f . In order to obtain a stable approximation of the fluid pressure also at the reduced order level, a supremizer enrichment may be necessary: the main reason for this is that, even if the FE spaces (V_h^f, Q_h) satisfy the inf-sup condition, this may not hold true anymore once we move to the reduced spaces generated by the reduced basis functions. To overcome this problem, we introduce the *supremizer variable* $s_h \in V_h^0$, which is defined by:

$$-(\operatorname{div}v_{f,h}, p_{f,h})_{\Omega_f} = (\nabla s_h, \nabla v_{f,h})_{\Omega_f} \quad \forall v_{f,h} \in V_h^0.$$

In the previous equation, $p_{f,h}$ is the FE pressure solution of the Navier–Stokes problem, whereas the right hand side is the H_0^1 scalar product, which we will consider for the velocity function space V_h^f . We refer the reader interested in more details on the supremizer enrichment technique to [1, 8]. Once we have obtained the FE supremizer snapshots s_h^i , $i = 0, \dots, N_T$, we are ready to generate a set of reduced basis; in order to do so, we decide to perform a Proper Orthogonal Decomposition on these snapshots: since the approach is monolithic, we try to preserve this structure also during the reduced basis generation. This means that we take the following correlation matrix \mathcal{C} :

$$\mathcal{C} := \operatorname{diag}(\mathcal{C}_u, \mathcal{C}_s, \mathcal{C}_p, \mathcal{C}_d^f, \mathcal{C}_d^s, \mathcal{C}_\lambda^u, \mathcal{C}_\lambda^d),$$

where:

$$\begin{aligned} (\mathcal{C}_u)_{ij} &:= (u_{0,h}^i, u_{0,h}^j)_{H^1} \quad i, j = 1 \dots, N_T \\ (\mathcal{C}_s)_{ij} &:= (s_h^i, s_h^j)_{H^1} \quad i, j = 1 \dots, N_T \\ (\mathcal{C}_p)_{ij} &:= (p_{f,h}^i, p_{f,h}^j)_{L^2} \quad i, j = 1 \dots, N_T \\ (\mathcal{C}_d^f)_{ij} &:= (d_{f,h}^i, d_{f,h}^j)_{H^1} \quad i, j = 1 \dots, N_T \\ (\mathcal{C}_d^s)_{ij} &:= (d_{s,h}^i, d_{s,h}^j)_{H^1} \quad i, j = 1 \dots, N_T \\ (\mathcal{C}_\lambda^u)_{ij} &:= (\lambda_{u,h}^i, \lambda_{u,h}^j)_{H^1} \quad i, j = 1 \dots, N_T \\ (\mathcal{C}_\lambda^d)_{ij} &:= (\lambda_{d,h}^i, \lambda_{d,h}^j)_{H^1} \quad i, j = 1 \dots, N_T. \end{aligned}$$

After performing an SVD on this matrix we end up with the following set of reduced basis: $\{\Phi_1^{s,u}, \dots, \Phi_{N_u}^{s,u}, \dots, \Phi_1^{\lambda_d}, \dots, \Phi_{N_{\lambda_d}}^{\lambda_d}\}$, where each basis function is a block function of six

components (one for each variable in the FSI problem):

$$\Phi_k^{s,u} = \begin{pmatrix} \Phi_k^{s,u} \\ 0 \\ 0 \\ 0 \\ 0 \end{pmatrix}, \dots, \Phi_k^{\lambda_d} = \begin{pmatrix} 0 \\ 0 \\ 0 \\ 0 \\ \Phi_k^{\lambda_d} \end{pmatrix}.$$

Here we have indicated $\Phi_k^{s,u}$ in order to remark the fact that the reduced basis functions for the fluid velocity consist of the reduced basis generated by the fluid velocity snapshots, to which we then add the reduced basis generated by the supremizer snapshots.

4.4. Online phase. Once we have the reduced basis functions, we can define the reduced solution $\mathbf{u}_N^{i+1} := (u_{0,N}^{i+1}, p_{f,N}^{i+1}, d_{f,N}^{i+1}, d_{s,N}^{i+1}, \lambda_{u,N}^{i+1}, \lambda_{d,N}^{i+1})$ of our FSI problem:

$$(8) \quad u_{0,N}^{i+1} := \sum_{k=0}^{N_u} \underline{u}_{0,k}^{i+1} \Phi_k^{s,u}$$

$$(9) \quad p_{f,N}^{i+1} := \sum_{k=0}^{N_p} \underline{p}_k^{i+1} \Phi_k^p$$

$$(10) \quad d_{f,N}^{i+1} := \sum_{k=0}^{N_{d_f}} \underline{d}_{f,k}^{i+1} \Phi_k^{d_f}$$

$$(11) \quad d_{s,N}^{i+1} := \sum_{k=0}^{N_{d_s}} \underline{d}_{s,k}^{i+1} \Phi_k^{d_s}$$

$$(12) \quad \lambda_{u,N}^{i+1} := \sum_{k=0}^{N_{\lambda_u}} \underline{\lambda}_{u,k}^{i+1} \Phi_k^{\lambda_u}$$

$$(13) \quad \lambda_{d,N}^{i+1} := \sum_{k=0}^{N_{\lambda_d}} \underline{\lambda}_{d,k}^{i+1} \Phi_k^{\lambda_d}.$$

In the previous equations the underline bar indicates the vector of coefficients of the reduced solution, therefore it indicates an element of \mathbb{R} (for scalar components of the reduced solution) or \mathbb{R}^2 for vectorial components of the reduced solution (such as the fluid velocity for example). The online monolithic reduced order system reads as follows: for every t^{i+1} , $i = 0, \dots, N_T - 1$, find $u_{0,N}^{i+1} \in V_N^0$, $p_{f,N}^{i+1} \in Q_N$, $d_{f,N}^{i+1} \in E_N^f$, $d_{s,N}^{i+1} \in E_N^s$, $\lambda_{u,N}^{i+1} \in L_N^u$ and $\lambda_{d,N}^{i+1} \in L_N^d$ such that for all $v_N \in V_N^0$, $q_N \in Q_N$, $e_N^f \in E_N^f$, $e_N^s \in E_N^s$, $\mu_N^u \in L_N^u$ and $\mu_N^d \in L_N^d$ it holds:

$$(14) \quad \begin{cases} (D_{tt} d_{s,N}^{i+1}, e_{s,N})_{\Omega_s} + (P(d_{s,N}^{i+1}), \nabla e_{s,h})_{\Omega_s} + (\lambda_{u,N}^{i+1}, e_{s,N})_{\Gamma_{FSI}} = 0, \\ \rho_f J(D_t(u_{0,N}^{i+1} + \ell_N), v_N)_{\Omega_f} + \rho_f J(\nabla(u_{0,N}^{i+1} + \ell_N) F^{-1}(u_{0,N}^{i+1} + \ell_N - D_t d_{f,N}^{i+1}), v_N)_{\Omega_f} + \\ + (J\sigma_f(u_{0,N}^{i+1} + \ell_N, p_{f,N}^{i+1}) F^{-T}, \nabla v_N)_{\Omega_f} - (\lambda_{u,N}^{i+1}, v_N)_{\Gamma_{FSI}} = 0, \\ -(\operatorname{div}(JF^{-1}u_{0,N}^{i+1} + \ell_N), q_N)_{\Omega_f} = 0 \\ (\frac{1}{J} \nabla d_{f,N}^{i+1}, \nabla e_{f,h})_{\Omega_f} = (\frac{1}{J} \lambda_{d,N}^{i+1}, e_{f,N})_{\Gamma_{FSI}}, \\ (u_{0,N}^{i+1} + \ell_N, \mu_{u,N})_{\Gamma_{FSI}} - (D_t d_{s,N}^{i+1}, \mu_{u,N})_{\Gamma_{FSI}} = 0, \\ (d_{f,N}^{i+1} - d_{s,N}^{i+1}, \mu_{d,N})_{\Gamma_{FSI}} = 0. \end{cases}$$

In the previous system ℓ_N is the projection of the Finite Element lifting function ℓ_h on the finite dimensional space generated by the velocity reduced basis functions.



FIGURE 1. Reference configuration of the benchmark test case. Solid is depicted in red, while the fluid domain is in blue.

5. RESULTS

We now present some numerical results that have been obtained adopting a monolithic approach for the Turek–Hron benchmark test case [48, 49]. Figure 1 represents the physical domain of the problem of interest. The channel has a length $L_f = 2.5$ cm and a height of $h_f = 0.41$ cm. The cylinder, which is assumed to be at rest and therefore is not considered as part of the solid domain, has center $C = (0.2, 0.2)$ and a radius of $r = 0.05$ cm. The deformable bar is 0.35 cm long and 0.02 cm thick.

TABLE 1. Values of the physical constants of the fluid and of the solid.

parameter	fluid	parameter	solid
$\rho_f [10^3 \frac{kg}{m^3}]$	1	$\rho_s [10^3 \frac{kg}{m^3}]$	1
$\nu_f [10^{-3} \frac{m^2}{s}]$	1	$\mu_s [10^6 \frac{kg}{ms^2}]$	0.5
$\bar{U} [\frac{m}{s}]$	1	ν_s	0.4

In Table 1 we have summarized the values of the physical parameters identifying the fluid and the solid behaviour: as we can see, the test case corresponds to a fluid with Reynolds number $Re = 100$. We impose homogeneous Dirichlet boundary conditions around the cylinder and on $\Gamma_{top \cup bottom}$ for the fluid velocity. We impose a velocity profile at the inlet boundary:

$$\bar{u}(t, x) := \begin{cases} \bar{U} \frac{1 - \cos(\frac{\pi}{2}t)}{2} & \text{if } t < 2s \\ \bar{U} & \text{otherwise,} \end{cases}$$

where

$$\bar{U}(y) = 1.5 \times \frac{4}{0.1681} y(0.41 - y).$$

We also require the bar to be attached to the cylinder, therefore $d_s = 0$ on Γ_D^s . We use a timestep $\Delta t = 10^{-2}$ for the discretization in time, and the two constants γ and β used for the discretization of the structure time derivatives have the following values: $\gamma = 0.25$ and $\beta = 0.5$. The total number of iterations of the simulation is $N_T = 10^3$. Since we are mostly interested in investigating the performance and the ability of the monolithic approach of reproducing the behaviour of the coupled system, we adopted a mixed approach: we use a standard FE method, until the elastic bar starts to oscillate and Karman vortexes appear in the fluid; then we run the reduced method. The oscillating behaviour of the system takes approximately $i = 800$ iterations to occur: we therefore run the monolithic reduced order method for the remaining 200 iterations. Figure 2 represents the behaviour of the first 100 eigenvalues obtained with the POD on the snapshots of the monolithic system.

Figure 3 represents the deformation of the elastic bar, at the final timestep of the simulation. The online solution has been obtained using $N_{d_s} = 20$ basis functions for the component d_s of the solution of the FSI system: as we can see, with this number of reduced basis the method is able to reconstruct precisely the behaviour of the solid component of the coupled system. In Figures 4 and 6 we can see the behaviour of the fluid pressure and of the fluid velocity respectively, again at the last timestep of the simulation: the FE solution is situated at the

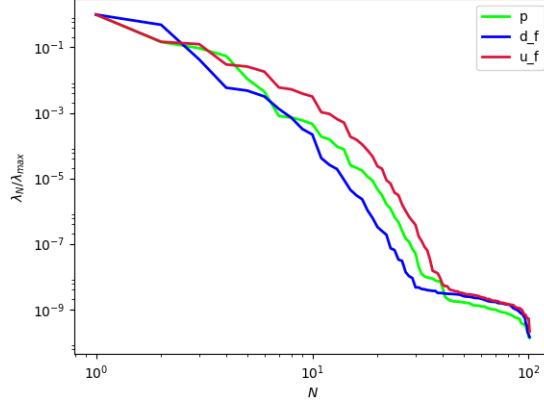


FIGURE 2. Eigenvalues decay for the fluid pressure p_f , the fluid velocity u_f and the mesh displacement d_f .

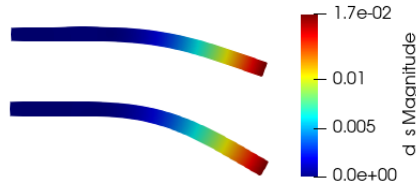


FIGURE 3. The deformation of the bar: the FE solution (top) and the reduced order solution (bottom). $N_{d_s} = 20$ basis functions have been used for the solid displacement. The deformation has been magnified by a factor 10 for visualization purposes.



FIGURE 4. Fluid pressure: the FE solution (top) and the reduced order solution (bottom). $N_p = 30$ basis functions have been used for the fluid pressure.

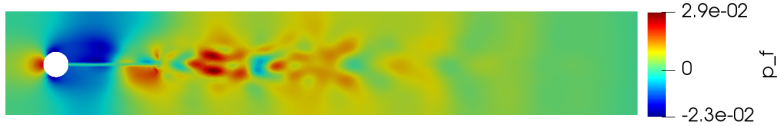


FIGURE 5. Fluid pressure approximation without the implementation of the supremizer enrichment: solution before the code diverges.

top, the reduced order approximation is at the bottom. As we can see in Figure 6, with a Reynolds number of 100, after some time we have the development of some Karman vortices that propagate into the fluid domain: the solid bar starts to oscillate and the whole system acquires a periodical behaviour. The monolithic algorithm is perfectly capable of capturing and reproducing these complex phenomena, such as the Karman vortices in the fluid. In Figure 4 the online approximation of the fluid pressure has been obtained by employing the supremizer enrichment technique, which requires the introduction of further basis functions

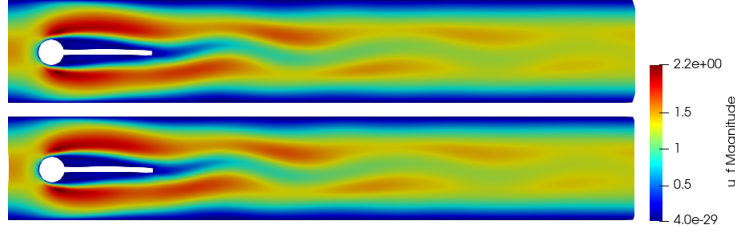


FIGURE 6. Fluid velocity: the FE solution (top) and the reduced order solution (bottom). $N_u = 60$ basis functions have been used for the fluid velocity.

in the fluid velocity reduced space: without this technique, the approximation of the fluid pressure becomes unstable and the whole algorithm diverges after a few timesteps, as we can see in Figure 5.

6. PARTITIONED APPROACH

In this Section we propose an alternative approach which is instead based on a segregated procedure: the idea is now to solve separately the fluid and the solid problem, and to couple the two physics through some iterative procedure. As we will see, this idea leads to some great advantages from the reduction point of view, and it also allows to work without the employment of additional Lagrange multipliers for the coupling conditions at the fluid–structure interface. The procedure that we propose is based on a Chorin–Temam projection scheme for the incompressible Navier–Stokes equations [27, 28]; in addition we employ a semi–implicit treatment of the coupling conditions ([5, 10, 22]).

6.1. Time discretization. We first present the partitioned scheme after time discretization. ΔT is the time–step: we employ also in this case an equispaced discretization of the time interval $[0, T]$. For the discretization of the time derivative of a function f we now use first backward difference BDF1:

$$D_t f^{i+1} = \frac{f^{i+1} - f^i}{\Delta T}, \quad D_{tt} f^{i+1} = D_t(D_t f^{i+1}).$$

The partitioned algorithm reads as follows: for $i = 0, \dots, N_T$:

- Extrapolation of the mesh displacement d_f : find $d_f^{i+1}: \Omega_f \mapsto \mathbb{R}^2$ such that:

$$(15) \quad \begin{cases} -\Delta d_f^{i+1} = 0 & \text{in } \Omega_f, \\ d_f^{i+1} = d_s^n & \text{on } \Gamma_{FSI}. \end{cases}$$

- Fluid explicit step: find $u_f^{i+1}: \Omega_f \mapsto \mathbb{R}^2$ such that:

$$(16) \quad \begin{cases} J\rho_f \left(\frac{u_f^{i+1} - u_f^i}{\Delta T} + \nabla u_f^{i+1} F^{-1}(u_f^{i+1} - D_t d_f^{i+1}) \right) - \\ \quad - \rho_f \nu_f \operatorname{div}(J\varepsilon(u_f^{i+1})F^{-T}) + JF^{-T} \nabla p_f^i = 0 & \text{in } \Omega_f, \\ u_f^{i+1} = D_t d_f^{i+1} & \text{on } \Gamma_{FSI}, \end{cases}$$

subject to the Dirichlet boundary condition $u_f^{i+1} = \bar{u}$ on Γ_D^f .

- Implicit step:

- (1) **fluid projection substep (pressure Poisson formulation):** find $p_f^{i+1}: \Omega_f \mapsto \mathbb{R}^2$ such that:

$$(17) \quad \begin{cases} -\frac{\rho_f}{\Delta t} \operatorname{div}(JF^{-1}u_f^{i+1}) = -\operatorname{div}(JF^{-1}F^{-T} \nabla p_f^{i+1}) & \text{in } \Omega_f, \\ -F^{-T} \nabla p_f^{i+1} \cdot JF^{-T} n_f = \rho_f D_{tt} d_s^{i+1} \cdot JF^{-T} n_f & \text{on } \Gamma_{FSI}, \end{cases}$$

subject to the boundary conditions:

$$(18) \quad p_f^{i+1} = \bar{p} \quad \text{on } \Gamma_D^f;$$

(2) **structure projection substep:** find $d_s^{i+1}: \Omega_s \mapsto \mathbb{R}^2$ such that:

$$(19) \quad \begin{cases} \rho_s D_{tt} d_s^{i+1} - \operatorname{div} P(d_s^{i+1}) = 0 & \text{in } \Omega_s, \\ J \sigma_f(u_f^{i+1}, p_f^{i+1}) F^{-T} n_f = -P(d_s^{i+1}) n_s & \text{on } \Gamma_{FSI}, \end{cases}$$

subject to the boundary condition $d_s^{i+1} = 0$ on Γ_D^s .

Before going any further, we briefly summarize some important remarks of this formulation of the original FSI problem:

- (1) The original Navier–Stokes problem has been divided into two subproblems, namely the fluid explicit step and the fluid projection step. In the explicit step, we take care of the viscous part of the fluid problem, whereas in the projection step we take care of the divergence free condition: this subdivision is a peculiarity of the Chorin–Temam projection scheme; we refer the interested reader to [27,28]. The advantage of adopting such a numerical scheme for the fluid problem is given by the fact that, in this case we can also use pairs of discrete spaces (V_h, Q_h) for the fluid velocity and pressure that do not necessary satisfy the inf–sup condition; this represents a great advantage for the forthcoming online phase of the method, since we are able to obtain stable approximation of the fluid pressure also without employing the supremizer enrichment technique, unlike in the monolithic approach.
- (2) The treatment of the boundary conditions is different for partitioned schemes: indeed now we have to give some boundary conditions also to the pressure Poisson problem, in order to have uniqueness of the solution. In this manuscript we decided to compute \bar{p} on Γ_D^f by extending the Navier–Stokes equation to the boundary of the fluid domain Ω_f , and by using the Dirichlet boundary condition for the fluid velocity, namely \bar{u} .
- (3) In the projection step (17) we choose a pressure Poisson formulation; it is possible to use a Darcy formulation instead: find p_f^{i+1} and \tilde{u}_f^{i+1} such that:

$$\begin{cases} \rho_f J \frac{\tilde{u}_f^{i+1} - u_f^{i+1}}{\Delta T} + J F^{-T} \nabla p_f^{i+1} = 0 & \text{in } \Omega_f, \\ \operatorname{div}(J F^{-1} \tilde{u}_f^{i+1}) = 0 & \text{in } \Omega_f. \end{cases}$$

However, in view of an efficient model order reduction, we choose to employ a Poisson formulation, since the Darcy formulation requires the introduction of an additional unknown \tilde{u}_f , which translates in a larger system, comprised of both velocity and pressure, at the implicit step.

In order to enhance the stability of the projection scheme, we employ a Robin–Neumann coupling, as proposed in [2,10]; for other references on this kind of coupling, we refer to [3,23]. We thus replace condition (17)₂ with the following:

$$(20) \quad \alpha_{ROB} p^{i+1} + F^{-T} \nabla p^{i+1} \cdot J F^{-T} n_f = \alpha_{ROB} p^{i+1,*} - \rho_f D_{tt} d_s^{i+1,*} \cdot J F^{-T} n_f.$$

In equation (20), $p^{i+1,*}$ and $d_s^{i+1,*}$ are suitable extrapolations of the fluid pressure and the solid displacement, respectively; we show in the next paragraph which kind of extrapolation we use. The constant α_{ROB} is defined as $\alpha_{ROB} = \frac{\rho_f}{z_p \Delta T}$ where z_p is called the *solid impedance*:

$$\begin{aligned} z_p &= \rho_s c_p, \\ c_p &= \sqrt{\frac{\lambda_s + 2\mu_s}{\rho_s}}. \end{aligned}$$

6.2. Space discretization. We now aim at giving the final formulation of the partitioned problem; in order to do so, we need to discretize in space the original problem. We consider hereafter the same function spaces V^f, V_0^f, E^f and E^s that have been defined in Section 4.2. For the fluid pressure we introduce, similarly to the fluid velocity, the following function

spaces:

$$\begin{aligned} Q &:= \{q \in L^2(\Omega_f) \text{ st. } q = \bar{p} \text{ on } \Gamma_D^f\}, \\ Q^0 &:= \{q \in L^2(\Omega_f) \text{ st. } q = 0 \text{ on } \Gamma_D^f\}. \end{aligned}$$

Also in this case we discretize in space the FSI problem, using second order Lagrange Finite Elements for the fluid velocity, the fluid displacement and the solid displacement, resulting in the discrete spaces $V_h^f \subset V^f$, $V_h^0 \subset V_0^f$, $E_h^f \subset E^f$ and $E_h^s \subset E^s$, while the fluid pressure is discretized with first order Lagrange Finite Elements, resulting in the discrete spaces $Q_h \subset Q$, $Q_h^0 \subset Q^0$. We are now ready to present the weak formulation of the original problem: for every $i = 0, \dots, N_T$,

- Extrapolation of the mesh displacement: find $d_{f,h}^{i+1} \in E_h^f$ such that $\forall e_{f,h} \in E_h^f$:

$$(21) \quad \begin{cases} (d_{f,h}^{i+1}, e_{f,h})_{\Omega_f} = 0 \\ d_{f,h}^{i+1} = d_{s,h}^n \quad \text{on } \Gamma_{FSI}. \end{cases}$$

- Fluid explicit step: find $u_{f,h}^{i+1} \in V_h^f$ such that $\forall v_h \in V_h^0$:

$$(22) \quad \begin{cases} \rho_f (J \left(\frac{u_{f,h}^{i+1} - u_{f,h}^n}{\Delta T} \right), v_h)_{\Omega_f} + \rho_f (J(\nabla u_{f,h}^{i+1} F^{-1}(u_{f,h}^{i+1} - D_t d_{f,h}^{i+1})), v_h)_{\Omega_f} \\ + \rho_f \nu_f (J \varepsilon(u_{f,h}^{i+1}) F^{-T}, \nabla v_h)_{\Omega_f} + (J F^{-T} \nabla p_{f,h}^n, v_h)_{\Omega_f} = 0 \\ u_{f,h}^{i+1} = D_t d_{f,h}^{i+1} \quad \text{on } \Gamma_{FSI}, \end{cases}$$

- Implicit step: for any $j = 0, \dots$ until convergence:

- (1) **fluid projection substep (pressure Poisson formulation):** find $p_{f,h}^{i+1,j+1} \in Q_h$ such that $\forall q_h \in Q_h^0$:

$$\begin{aligned} & - \frac{\rho_f}{\Delta T} (\text{div}(J F^{-1} u_{f,h}^{i+1}), q_h)_{\Omega_f} - \rho_f ((D_{tt} d_{s,h}^{i+1,j}), J F^{-T} n_f q_h)_{\Gamma_{FSI}} \\ & + \alpha_{ROB} (p_{f,h}^{i+1,j}, q_h)_{\Gamma_{FSI}} = \\ & = \alpha_{ROB} (p_{f,h}^{i+1,j+1}, q_h)_{\Gamma_{FSI}} + (J F^{-T} \nabla p_{f,h}^{i+1,j+1}, F^{-T} \nabla q_h)_{\Omega_f}. \end{aligned}$$

- (2) **structure projection substep:** find $d_{s,h}^{i+1,j+1} \in E_h^s$ such that $\forall e_{s,h} \in E_h^s$:

$$\begin{aligned} & \rho_s (D_{tt} d_{s,h}^{i+1,j+1}, e_{s,h})_{\Omega_f} + (P(d_{s,h}^{i+1,j+1}), \nabla e_{s,h})_{\Omega_s} = \\ & = -(J \sigma_f(u_{f,h}^{i+1}, p_{f,h}^{i+1,j+1}) F^{-T} n_f, e_{s,h})_{\Omega_s} \end{aligned}$$

subject to the boundary condition $d_{s,h}^{i+1,j+1} = 0$ on Γ_D^s

We iterate between the two implicit substeps, using a fixed point strategy:

$$\max \left(\frac{\|p_{f,h}^{i+1,j+1} - p_{f,h}^{i+1,j}\|_{Q_h}}{\|p_{f,h}^{i+1,j+1}\|_{Q_h}}; \frac{\|d_{s,h}^{i+1,j+1} - d_{s,h}^{i+1,j}\|_{E_h^s}}{\|d_{s,h}^{i+1,j+1}\|_{E_h^s}} \right) < \varepsilon,$$

where ε is a fixed tolerance.

In the pressure Poisson formulation, to impose the Robin coupling condition, we have chosen the pressure at the previous implicit iteration, namely $p_f^{i+1,j}$, as an extrapolation for the fluid pressure, and the same goes for the extrapolation of the structure displacement.

6.3. Reduced Basis generation. For the generation of the reduced basis for the fluid velocity $u_{f,h}$ and the fluid displacement $d_{f,h}$ we pursue here the idea that was first proposed in [10]. For the solid displacement $d_{s,h}$ we employ a standard POD; for fluid pressure $p_{f,h}$ we first introduce a lifting function ℓ^p and obtain the homogenized pressure $p_{0,h} = p_{f,h} - \ell^p$ such that $p_{0,h} = 0$ on Γ_D^f , and then we perform a standard POD.

6.3.1. *Change of variable for the fluid velocity.* The main idea here is to introduce a change of variable in the fluid problem, in order to transform condition $(22)_2$ into a homogeneous boundary condition. The motivation of this choice is that, to impose condition $(22)_2$, we could use a Lagrange multiplier λ , but unfortunately introducing a new variable leads to an increased dimension of the system to be solved in the online phase. Therefore, in order to avoid this and in order to design a more efficient reduced method, we choose to transform the non-homogeneous coupling condition into a homogeneous one. First of all we introduce a lifting function ℓ^u , similarly to what has been done for the monolithic approach in Section 4.3: we therefore obtain a homogenized fluid velocity $u_{0,h}^{i+1}$ such that $u_{0,h}^{i+1} = 0$ on Γ_D^f . Afterwards we define a new variable $z_{f,h}^{i+1}$:

$$z_{f,h}^{i+1} := u_{0,h}^{i+1} - D_t d_{f,h}^{i+1}.$$

With this change of variable, equation $(22)_2$ is equivalent to the homogeneous boundary condition for the new variable:

$$z_{f,h}^{i+1} = 0 \quad \text{on } \Gamma_{FSI},$$

for which no imposition by means of Lagrange multiplier is needed. Therefore, during the offline phase of the scheme, at every iteration $i + 1$, after we have computed the homogenized velocity $u_{0,h}^{i+1}$, we compute the change of variable $z_{f,h}^{i+1}$. We then consider the following snapshots matrix:

$$\mathcal{S}_z = [z_{f,h}^1, \dots, z_{f,h}^{N_T}] \in \mathbb{R}^{\mathcal{N}_u^h \times N_T},$$

where $\mathcal{N}_u^h = \dim V_h$ and we use the underline notation to denote the vector consisting of the FE degrees of freedom corresponding to each solution. We then apply a POD to the snapshots matrix \mathcal{S}_z and we retain the first N_z POD modes $\Phi_z^1, \dots, \Phi_z^{N_z}$. We therefore have the reduced space:

$$V^N := \text{span}\{\Phi_z^k\}_{k=1}^{N_z},$$

and now it is clear that, since every Φ_z^k satisfies the condition $\Phi_z^k = 0$ on Γ_{FSI} , then also every element of V^N will satisfy the same condition.

6.3.2. *Harmonic extension of the fluid displacement.* In order to generate the reduced basis for the fluid displacement d_f , we pursue again the idea presented in [10]. Therefore, we start by generating the snapshots matrix related to the solid displacement:

$$\mathcal{S}_{d_s} = [\underline{d}_{s,h}^1, \dots, \underline{d}_{s,h}^{N_T}] \in \mathbb{R}^{\mathcal{N}_{d_s}^h \times N_T},$$

where $\mathcal{N}_{d_s}^h = \dim E_h^s$ and again the underline notation denotes the vector of the FE degrees of freedom corresponding to each solution of the solid displacement. We then apply a POD to the snapshots matrix and retain the first N_{d_s} POD modes $\Phi_{d_s}^1, \dots, \Phi_{d_s}^{N_{d_s}}$, thus defining the reduced space for the solid problem:

$$E_N^s := \text{span}\{\Phi_{d_s}^k\}_{k=1}^{N_{d_s}}.$$

We then employ an harmonic extension of each one of the reduced basis $\Phi_{d_s}^k$ to the fluid domain, thus obtaining the functions $\Phi_{d_f}^k$ such that:

$$\begin{cases} -\Delta \Phi_{d_f}^k = 0 & \text{in } \Omega_f, \\ \Phi_{d_f}^k = \Phi_{d_s}^k & \text{on } \Gamma_{FSI}. \end{cases}$$

We can then define the reduced space for the fluid displacement:

$$E_N^f := \text{span}\{\Phi_{d_f}^k\}_{k=1}^{N_{d_s}}.$$

The reason for defining the basis functions for d_f in such a way, instead of employing a standard POD on the set of snapshots for the fluid displacement computed in the offline phase relies in the fact that we want to avoid the introduction of another Lagrange multiplier to impose the non-homogeneous boundary condition $(21)_2$. With our method, we avoid to solve the reduced system related to (21): indeed, instead of solving an harmonic extension problem at every

time-step in the online phase, we solve *once and for all* N_{d_s} harmonic extension problems in the expensive offline phase. Then, during the online phase, the reduced fluid displacement will be computed just as a linear combination of the basis $\Phi_{d_f}^i$, with coefficients that are the coefficients of the reduced solid displacement at the previous time-step. We will see in the next Section the final formulation of the online phase of the algorithm.

6.4. Online computational phase. We are now ready to present the online formulation of the partitioned procedure. For every $i = 0, \dots, N_T$, we introduce the reduced functions $z_{f,N}^{i+1}$, $p_{f,N}^{0,i+1}$, $d_{s,N}^{i+1}$ of the form:

$$(23) \quad z_{f,N}^{i+1} = \sum_{k=1}^{N_{z_f}} \underline{z}_k^{i+1} \Phi_{z_f}^k,$$

$$(24) \quad p_{f,N}^{0,i+1} = \sum_{k=1}^{N_p} \underline{p}_k^{0,i+1} \Phi_p^k,$$

$$(25) \quad d_{s,N}^{i+1} = \sum_{k=1}^{N_{d_s}} \underline{d}_k^{i+1} \Phi_{d_s}^k.$$

Then the online phase of the partitioned procedure reads as follows:

Mesh displacement: let $d_{f,N}^{i+1}$ be defined by the reduced solid displacement at the previous time-step:

$$(26) \quad d_{f,N}^{i+1} = \sum_{k=1}^{N_{d_s}} \underline{d}_k^i \Phi_{d_f}^k;$$

Fluid explicit step (with change of variable): find $z_{f,N}^{i+1} \in V_N$ such that $\forall v_N \in V_N$:

$$\begin{aligned} & \rho_f \int_{\Omega_f} J \left(\frac{z_{f,N}^{i+1} - u_{f,N}^i}{\Delta T} \right) \cdot v_N \, dx + \rho_f \int_{\Omega_f} J (\nabla (z_{f,N}^{i+1} + D_t d_{f,N}^{i+1}) F^{-1} z_{f,N}^{i+1}) \cdot v_N \, dx \\ & + \mu_f \int_{\Omega_f} J \varepsilon (z_{f,N}^{i+1}) F^{-T} : \nabla v_N \, dx + \int_{\Omega_f} J F^{-T} \nabla p_{f,N}^i \cdot v_h \, dx = \\ & - \rho_f \int_{\Omega_f} J \left(\frac{D_t d_{f,N}^{i+1}}{\Delta T} \right) \cdot v_N \, dx - \mu_f \int_{\Omega_f} J \varepsilon (D_t d_{f,N}^{i+1}) F^{-T} : \nabla v_N \, dx \quad \text{in } \Omega_f. \end{aligned}$$

We then restore the reduced fluid velocity: $u_{f,N}^{i+1} = z_{f,N}^{i+1} + D_t d_{f,N}^{i+1}$.

Implicit step: for any $j = 0, \dots$ until convergence:

(1) **fluid projection substep:** find $p_{f,N}^{0,i+1,j+1} \in Q_N^0$ such that $\forall q_N \in Q_N^0$:

$$\begin{aligned} & - \frac{\rho_f}{\Delta T} \int_{\Omega_f} \operatorname{div} (J F^{-1} u_{f,N}^{i+1}) q_N \, dx - \rho_f \int_{\Gamma_{FSI}} (D_{tt} d_{s,N}^{i+1,j}) \cdot J F^{-T} n_f q_N \, ds \\ & + \alpha_{ROB} \int_{\Gamma_{FSI}} p_{f,N}^{i+1,j} q_N \, ds - \alpha_{ROB} \int_{\Gamma_{FSI}} \ell^{i+1} q_N \, ds \\ & - \int_{\Omega_f} J F^{-T} \nabla \ell^{i+1} \cdot F^{-T} \nabla q_N \, dx = \alpha_{ROB} \int_{\Gamma_{FSI}} p_{f,N}^{i+1,j+1} q_N \, ds \\ & + \int_{\Omega_f} J F^{-T} \nabla p_{f,N}^{i+1,j+1} \cdot F^{-T} \nabla q_N \, dx; \end{aligned}$$

we then recover the reduced fluid pressure $p_{f,N}^{i+1,j+1} = p_{f,N}^{0,i+1,j+1} + \ell^{i+1}$.

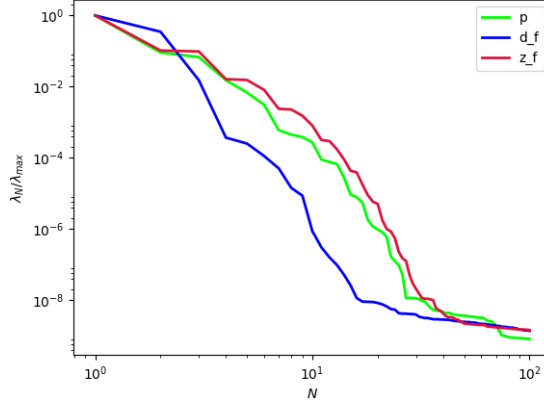


FIGURE 7. Decay of the eigenvalues of the fluid pressure p_f , the change of variable z_f and the mesh displacement d_f .

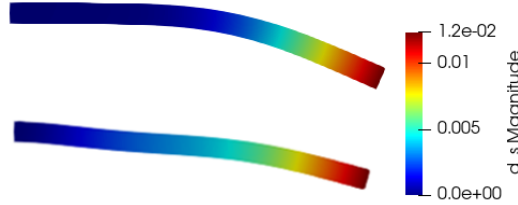


FIGURE 8. Deformation of the structure: FE solution (top) and reduced order solution (bottom). The approximation has been obtained with $N_{d_s} = 20$ basis functions. The deformation has been magnified by a factor 10 for visualization purposes.

(2) **structure projection substep:** find $d_{s,N}^{i+1,j+1} \in E_N^s$ such that $\forall e_s \in E_N^s$:

$$\begin{aligned} \rho_s \int_{\Omega_s} D_{tt} d_{s,N}^{i+1,j+1} \cdot e_N \, dx + \int_{\Omega_s} P(d_{s,N}^{i+1,j+1}) : \nabla e_N \, dx &= \\ &= - \int_{\Omega_s} J \sigma_f(u_{f,N}^{i+1}, p_{f,N}^{i+1,j+1}) F^{-T} n_f \cdot e_N \, dx \end{aligned}$$

7. RESULTS

We now present some results obtained by implementing the partitioned algorithm previously described for the same FSI test case, namely the Turek–Hron benchmark test case. The physical constants describing the fluid and the solid properties are the same, and we therefore refer to the values of Table 1.

The timestep used for the segregated approach is $\Delta t = 10^{-3}$, for a total of $N_T = 10^4$ iterations. Also in this case, we adopt a standard FE approach for the first 8000 iterations, and we employ the partitioned reduced order model for the remaining 2000 iterations.

Figure 7 show the rate of decay of the eigenvalues for the fluid pressure p_f , the mesh displacement d_f and the fluid velocity change of variable z_f . In Figure 8 we can see the deformation of the elastic beam, at the last timestep of the simulation: also in this case, with just 20 basis functions the reduced order approach is able to reproduce quite accurately the behaviour of the solid. Figure 9 shows the fluid pressure, that in the partitioned scheme has been obtained by solving a Poisson problem: this clearly leads to numerical results that are slightly different from the ones in the monolithic approach, but this has to be expected, since we introduced a "fictitious" Dirichlet boundary condition for the fluid pressure, in order to guarantee uniqueness of the solution of the Poisson problem. As we can see, the reduced order fluid pressure represents accurately the FE snapshot, even without the use of the supremizer



FIGURE 9. Pressure Poisson recovery: FE solution (top) and reduced order solution (bottom). The approximation has been obtained with $N_{p_f} = 20$ basis functions.

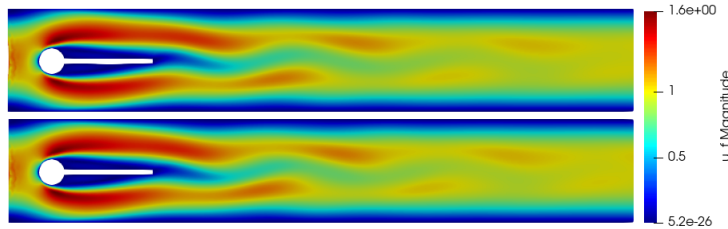


FIGURE 10. Fluid velocity: FE solution (top) and reduced order solution (bottom). The approximation has been obtained with $N_{u_f} = 20$ basis functions.

enrichment technique. Finally in Figure 10 we can see the behaviour of the fluid velocity: also in this case we recognise the Karman vortexes that develop after a while; we remark that the fluid velocity in the figure is just the solution of the viscous part of the Navier–Stokes equation, since we employed the Chorin–Temam projection scheme also in the reduced order model.

8. DISCUSSION

We applied two different model order reduction approaches to a benchmark test case of interest, namely the Turek–Hron FSI test case. The aim of the work was that of building a report and an analysis of the performance of the two most used approaches in the fluid–structure interaction community, namely partitioned and monolithic algorithms.

TABLE 2. A comparison between the two approaches

Monolithic approach	Value
ΔT	0.01 s
number of iterations of the RB solver	200
computational time cost	40 min
dimension of the whole online system	150×150
Partitioned approach	Value
ΔT	0.001 s
number of iterations of the RB solver	2000
computational time cost	2 hours
dimension of the online system for the fluid viscous part	20×20
dimension of the online system for the pressure Poisson part	20×20
dimension of the online system for the solid problem	20×20

In Table 2 we have summarized some important aspects of both the reduction procedures, in order to highlight the differences of the two approaches. All the numerical simulations

have been performed on a computer with 3.50 GHz per CPU, and the mesh used in the two approaches is the same.

The monolithic algorithm, as we have seen, brings along an increase in the number of unknowns to be used in the coupled system: this is because, in order to impose the coupling conditions, we used two Lagrange multipliers, and this leads to an increase in the dimension of the algebraic system to be solved during the online phase. In addition to this, in order to obtain a stable approximation of the reduced order fluid pressure, we adopted a supremizer enrichment of the reduced fluid velocity space: this also leads to an increase of the number of basis functions to be used in the online phase, with a further increase of the dimension of the algebraic system. On the other hand, a monolithic approach is more stable, and therefore allows for bigger time steps in the numerical simulations: this turns out to be extremely useful, especially in the case of physical phenomena which take some time to develop, such as the Karman vortexes in the Turek–Hron benchmark that we considered.

The partitioned algorithm is very useful, and it gives a lot of control on the systems to be solved during the online phase of the reduction method. In this work we chose a semi-implicit treatment of the coupling conditions: this is, in our opinion, the best choice for the test case considered. Indeed, an implicit treatment of the coupling conditions would be too expensive, and would drastically increase the number of sub-iterations at each time step, both in the offline phase and in the online phase. We also tried to adopt an explicit treatment of the coupling conditions, as suggested for example in [21]: this approach is unstable for the benchmark considered here, because, due to the slender shape of the domain, the added mass effect plays an important role, and leads to an algorithm that diverges after a few timesteps. Therefore the implicit coupling is the best tradeoff between stability and computational cost. The Chorin–Temam projection scheme has allowed us to work without the need of a supremizer enrichment technique: this gives a good control on the number of basis functions to be used in the online phase of the method. In addition to this, the choice of a pressure Poisson formulation allows us to discard the so called *end of step* velocity, and to work just with the intermediate velocity, leading again to a decrease in the dimension of the online system. Finally, the harmonic extension of the fluid displacement basis functions gives the possibility to efficiently compute the mesh displacement in the online phase of the method, without the need of solving an additional system. The drawback of a partitioned reduced order model, as we have seen in the numerical results section, is that the timestep required in order to have a stable algorithm is, in general, much smaller with respect to the timestep that can be used in a monolithic approach, thus resulting in a larger number of snapshots to be processed in the offline phase. In addition to this, the treatment of the boundary conditions is rather delicate with partitioned approaches, and it needs to be tailored to the problem at hand, whereas with a monolithic approach the imposition of these conditions is simpler, either by incorporating them in the weak formulation or by using Lagrange multipliers.

9. CONCLUSIONS

We conclude this work by saying that, from the reduced order point of view, both a monolithic approach as well as a partitioned approach have many advantages and few disadvantages. For long time simulations, such as the one considered in this manuscript, we would advise to use a monolithic approach: even though we are introducing a few new variables in the problem formulation, we can still make the entire approach computationally feasible: for example, a suggestion could be to perform a rather sparse Proper Orthogonal Decomposition on the first snapshots (when the important physical phenomenon, such as the Karman vortexes in our test case, is not yet developed), and then refine the sampling. We are aware that this requires some sort of "a priori" knowledge of the physical phenomenon that we are simulating: for the benchmark test case considered, plenty of numerical results already exist that can provide an insight on when to refine the sampling procedure. For other applications, this opens up the possibility of bridging a monolithic reduction procedure with some machine learning algorithm

that can be used to investigate, in an efficient way, the overall behaviour of the solution to be approximated.

As long as the partitioned approach concerns, its application is very well indicated for those problems which do not require long time simulations, and for industrial applications, since the idea of a segregated algorithm is to combine already existing, at the state of the art softwares for computational fluid dynamics and computational solid mechanics. Nonetheless, until alternative stopping criteria and/or alternative treatments of the coupling conditions are further investigated, their application to long time simulations results in an increase of the computational time also during the online phase.

ACKNOWLEDGEMENTS

We acknowledge the support by European Union Funding for Research and Innovation â€“ Horizon 2020 Program â€“ in the framework of European Research Council Executive Agency: Consolidator Grant H2020 ERC CoG 2015 AROMA-CFD project 681447 ”Advanced Reduced Order Methods with Applications in Computational Fluid Dynamics” (PI Prof. Gianluigi Rozza). We also acknowledge the INDAM-GNCS project ”Tecniche Numeriche Avanzate per Applicazioni Industriali”. Numerical simulations have been obtained with the extension multiphenics of FEniCS [2, 35] for the high fidelity part, and RBniCS [1] for the reduced order part. We acknowledge developers and contributors of each of the aforementioned libraries. Dr. Nonino acknowledges also the support of the Austrian Science Fund (FWF) project F65 ”Taming complexity in Partial Differential Systems” and the Austrian Science Fund (FWF) project P 33477.

REFERENCES

1. S. Ali, F. Ballarin, and G. Rozza, *Stabilized reduced basis methods for parametrized steady Stokes and Navier-Stokes equations*, Computers & Mathematics with Applications (2020).
2. M. Astorino, F. Chouly, and M. A. Fernández, *Robin based semi-implicit coupling in Fluid-Structure Interaction: stability analysis and numerics*, SIAM Journal on Scientific Computing **31** (2010), no. 6, 4041–4065.
3. S. Badia, F. Nobile, and C. Vergara, *Fluid-structure partitioned procedures based on Robin transmission conditions*, Journal of Computational Physics **227** (2008), no. 14, 7027 – 7051.
4. S. Badia, A. Quaini, and A. Quarteroni, *Modular vs. non-modular preconditioners for fluid-structure systems with large added-mass effect*, Computer Methods in Applied Mechanics and Engineering **197** (2008), no. 49, 4216 – 4232.
5. S. Badia, A. Quaini, and A. Quarteroni, *Splitting methods based on algebraic factorization for Fluid-Structure Interaction*, SIAM Journal on Scientific Computing **30** (2008), no. 4, 1778–1805.
6. S. Badia, A. Quaini, and A. Quarteroni, *Coupling Biot and Navier-Stokes equations for modelling fluid-poroelastic media interaction*, Journal of Computational Physics **228** (2009), no. 21, 7986 – 8014.
7. F. Ballarin, E. Faggiano, S. Ippolito, Manzoni, A. Quarteroni, G. Rozza, and R. Scrofani, *Fast simulations of patient-specific haemodynamics of coronary artery bypass grafts based on a POD-Galerkin method and a vascular shape parametrization*, Journal of Computational Physics **315** (2016), 609–628.
8. F. Ballarin, A. Manzoni, A. Quarteroni, and G. Rozza, *Supremizer stabilization of POD-Galerkin approximation of parametrized steady incompressible Navier-Stokes equations*, International Journal for Numerical Methods in Engineering **102** (2015), no. 5, 1136–1161.
9. F. Ballarin and G. Rozza, *POD-Galerkin monolithic reduced order models for parametrized Fluid-Structure Interaction problems*, International Journal for Numerical Methods in Fluids **82** (2016), no. 12, 1010–1034.
10. F. Ballarin, G. Rozza, and Y. Maday, *Reduced-order semi-implicit schemes for Fluid-Structure Interaction problems*, Model Reduction of Parametrized Systems (P. Benner, M. Ohlberger, A. T. Patera, G. Rozza, and K. Urban, eds.), MS&A series, vol. 17, Springer, Cham., 2017, pp. 149–167.
11. S. Basting, A. Quaini, S. Čanić, and R. Glowinski, *Extended ALE method for Fluid-Structure Interaction problems with large structural displacements*, Journal of Computational Physics **331** (2017), 312 – 336.
12. L. Bertagna and A. Veneziani, *A model reduction approach for the variational estimation of vascular compliance by solving an inverse Fluid-Structure Interaction problem*, Inverse Problems **30** (2014), no. 5, 055006.
13. M. Bukač, S. Čanić, R. Glowinski, J. Tambača, and A. Quaini, *Fluid-Structure Interaction in blood flow capturing non-zero longitudinal structure displacement*, Journal of Computational Physics **235** (2013), 515 – 541.

14. E. Burman, S. Claus, P. Hansbo, M. Larson, and A. Massing, *CutFEM: discretizing geometry and partial differential equations*, International Journal for Numerical Methods in Engineering **104** (2014), 472–501.
15. E. Burman and P. Hansbo, *Fictitious domain methods using cut elements: III. a stabilized Nitsche method for Stokes’ problem*, ESAIM: Mathematical Modelling and Numerical Analysis - Modélisation Mathématique et Analyse Numérique **48** (2014), no. 3, 859–874.
16. P. Causin, J. F. Gerbeau, and F. Nobile, *Added-mass effect in the design of partitioned algorithms for fluid–structure problems*, Computer Methods in Applied Mechanics and Engineering **194** (2005), no. 42, 4506 – 4527.
17. V. Chabannes, G. Pena, and Prud’homme C., *High–order fluid–structure interaction in 2d and 3d application to blood flow in arteries*, Journal of Computational and Applied Mathematics **246** (2013), 1–9.
18. A. Derkevorkian, P. Avery, C. Farhat, J. Rabinovitch, and L. Peterson, *Effects of structural parameters on the FSI simulation of supersonic parachute deployments*, AIAA Aviation 2019 Forum, Dallas, Texas.
19. D. Errate, M. J. Esteban, and Y. Maday, *Couplage fluid–structure. Un modele simplifié en dimension 1.*, Comptes rendus de l’Académie des sciences. Série 1, Mathématique **318** (1994), 275–281.
20. C. Farhat and V. K. Lakshminarayan, *An ALE formulation of embedded boundary methods for tracking boundary layers in turbulent Fluid–Structure Interaction problems*, Journal of Computational Physics **263** (2014), 53 – 70.
21. C. Farhat, K. G. van der Zee, and P. Geuzaine, *Provably second-order time-accurate loosely-coupled solution algorithms for transient nonlinear computational aeroelasticity*, Computer Methods in Applied Mechanics and Engineering **195** (2006), no. 17, 1973 – 2001.
22. M. A. Fernández, J. F. Gerbeau, and C. Grandmont, *A projection semi-implicit scheme for the coupling of an elastic structure with an incompressible fluid*, International Journal for Numerical Methods in Engineering **69** (2007), no. 4, 794–821.
23. M. A. Fernández, J. Mullaert, and M. Vidrascu, *Explicit Robin–Neumann schemes for the coupling of incompressible fluids with thin-walled structures*, Computer Methods in Applied Mechanics and Engineering **267** (2013), 566 – 593.
24. D. Forti, M. Bukac, A. Quaini, S. Čanić, and S. Deparis, *A Monolithic Approach to Fluid–Composite Structure Interaction*, Journal of Scientific Computing **72** (2017), no. 1, 396–421.
25. M. W. Gee, U. Küttler, and W. A. Wall, *Truly monolithic algebraic multigrid for fluid–structure interaction*, International Journal for Numerical Methods in Engineering **85** (2011), no. 8, 987–1016.
26. C. Grandmont and Y. Maday, *Existence de solutions d’un problème de couplage fluide-structure bidimensionnel instationnaire*, Comptes Rendus de l’Académie des Sciences - Series I - Mathematics **326** (1998), no. 4, 525 – 530.
27. J. L. Guermond and L. Quartapelle, *Calculation of incompressible viscous flows by an unconditionally stable projection fem*, Journal of Computational Physics **132** (1997), no. 1, 12 – 33.
28. J. L. Guermond and L. Quartapelle, *On the approximation of the unsteady navier–stokes equations by finite element projection methods*, Numerische Mathematik **80** (1998), 207–238.
29. B. Haasdonk, *Reduced basis methods for parametrized PDEs – a tutorial introduction for stationary and instationary problems*, Model Reduction and Approximation: theory and algorithms (P. Benner, A. Cohen, M. Ohlberger, and K. Willcox, eds.), Computational science and engineering, Siam, Philadelphia, 2017, pp. 65–136.
30. B. Haasdonk and M. Ohlberger, *Reduced basis method for finite volume approximations of parametrized linear evolution equations*, ESAIM: M2AN **42** (2008), no. 2, 277–302.
31. J. S. Hesthaven, G. Rozza, and B. Stamm, *Certified reduced basis methods for parametrized partial differential equations*, Springer Briefs in Mathematics, Springer Cham Heidelberg New York Dordrecht London, 2016.
32. J. F. Gerbeau and M. Vidrascu, *A quasi-Newton algorithm based on a reduced model for Fluid–Structure Interaction problems in blood flows*, ESAIM: M2AN **37** (2003), no. 4, 631–647.
33. E. Karatzas, M. Nonino, F. Ballarin, and G. Rozza, *A Reduced Order Cut Finite Element Method for geometrically parametrized steady and unsteady Navier–Stokes*, submitted, 2020.
34. T. Lassila, A. Manzoni, A. Quarteroni, and G. Rozza, *Model order reduction in fluid dynamics: challenges and perspectives*, Reduced Order Methods for Modeling and Computational Reduction (A. Quarteroni and G. Rozza, eds.), MS&A series, vol. 9, Springer, Cham., 2014, pp. 235–273.
35. P. Le Tallec and J. Mouro, *Fluid structure interaction with large structural displacements*, Computer Methods in Applied Mechanics and Engineering **190** (2001), no. 24, 3039 – 3067, Advances in Computational Methods for Fluid–Structure Interaction.
36. T. Lieu, C. Farhat, and M. Lesoinne, *Reduced-order fluid/structure modeling of a complete aircraft configuration*, Computer Methods in Applied Mechanics and Engineering **195** (2006), no. 41, 5730 – 5742.
37. M. Lombardi, N. Parolini, A. Quarteroni, and G. Rozza, *Numerical simulation of sailing boats: dynamics, FSI, and shape optimization*, Variational Analysis and Aerospace Engineering: Mathematical Challenges for Aerospace Design (G. Buttazzo and A. Frediani, eds.), Springer Optimization and its Applications, vol. 66, Springer, Boston, MA, 2012, pp. 339–377.

38. Y. Maday, *Analysis of coupled models for fluid-structure interaction of internal flows*, Cardiovascular Mathematics: Modeling and simulation of the circulatory system (L. Formaggia, A. Quarteroni, and A. Veneziani, eds.), Springer Milan, 2009, pp. 279–306.
39. N. C. Nguyen, G. Rozza, and A. T. Patera, *Reduced basis approximation and a posteriori error estimation for the time-dependent viscous Burgers' equation*, *Calcolo* **46** (2009), no. 3, 157–185.
40. M. Nonino, F. Ballarin, G. Rozza, and Y. Maday, *Overcoming slowly decaying Kolmogorov n -width by transport maps: application to model order reduction of fluid dynamics and Fluid–Structure Interaction problems*, arXiv:1911.06598, 2019.
41. S. Piperno and C. Farhat, *Design of efficient partitioned procedures for the transient solution of aeroelastic problems*, *Revue Européenne des Éléments Finis* **9** (2000), no. 6-7, 655–680.
42. A. Quaini, *Algorithms for Fluid–Structure Interaction problems arising in hemodynamics*, Ph.D. thesis, EPFL, Lausanne, 2009.
43. A. Quarteroni and L. Formaggia, *Mathematical modelling and numerical simulation of the cardiovascular system*, *Handbook of Numerical Analysis* **12** (2004), 3–127.
44. A. Quarteroni, M. Tuveri, and A. Veneziani, *Computational vascular fluid dynamics: problems, models and methods*, *Computing and Visualization in Science* **2** (2000), 163–197.
45. J. Rabinovitch, D. Z. Huang, R. Borker, P. Avery, C. Farhat, A. Derkevorkian, and L. Peterson, *Towards a validated fsi computational framework for supersonic parachute deployments*, AIAA Aviation 2019 Forum.
46. T. Richter, *Fluid–structure interactions. model, analysis and finite element*, *Lecture Notes in Computational Science and Engineering*, vol. 118, Springer International Publishing, 2017.
47. G. Rozza, D. B. P. Huynh, and A. T. Patera, *Reduced basis approximation and a posteriori error estimation for affinely parametrized elliptic coercive partial differential equations: Application to transport and continuum mechanics*, *Archives of Computational Methods in Engineering* **15** (2008), no. 3, 229–275.
48. S. Turek and J. Hron, *Proposal for numerical benchmarking of fluid-structure interaction between an elastic object and laminar incompressible flow*, *Fluid-Structure Interaction* (Berlin, Heidelberg) (Hans-Joachim Bungartz and Michael Schäfer, eds.), Springer Berlin Heidelberg, 2006, pp. 371–385.
49. S. Turek, J. Hron, M. Razzaq, H. Wobker, and M. Schäfer, *Numerical benchmarking of fluid-structure interaction: A comparison of different discretization and solution approaches*, *Fluid Structure Interaction II* (Berlin, Heidelberg) (Hans-Joachim Bungartz, Miriam Mehl, and Michael Schäfer, eds.), Springer Berlin Heidelberg, 2010, pp. 413–424.
50. W. Q. Wang and Y. Yan, *Strongly coupling of partitioned fluid–solid interaction solvers using reduced-order models*, *Applied Mathematical Modelling* **34** (2010), no. 12, 3817 – 3830.
51. Y. Wang, A. Quaini, and S. Čanić, *A higher-order discontinuous galerkin/arbitrary lagrangian eulerian partitioned approach to solving fluid–structure interaction problems with incompressible, viscous fluids and elastic structures*, *Journal of Scientific Computing* **76** (2018), 481–520.
52. Y. Wang, A. Quaini, S. Čanić, M. Vukicevic, and S. H. Little, *3d experimental and computational analysis of eccentric mitral regurgitant jets in a mock imaging heart chamber*, *Cardiovascular Engineering and Technology* **8** (2017), no. 4, 419–438.
53. Y. Wu and X. C. Cai, *A fully implicit domain decomposition based ALE framework for three-dimensional Fluid–Structure Interaction with application in blood flow computation*, *Journal of Computational Physics* **258** (2014), 524 – 537.